UC Berkeley
UC Berkeley Previously Published Works

Title

Performance Assessment for Geological Disposal of Graphite Waste Containing TRISO Particles

Permalink

https://escholarship.org/uc/item/2xr2t925

Journal

Nuclear Technology, 181(3)

Authors

van den Akker, Bret Patrick
Ahn, Joonhong

Publication Date

2013-03-01

Peer reviewed

PERFORMANCE ASSESSMENT FOR GEOLOGICAL DISPOSAL OF GRAPHITE WASTE CONTAINING TRISO PARTICLES

BRET PATRICK VAN DEN AKKER and JOONHONG AHN*

University of California at Berkeley, Department of Nuclear Engineering
Berkeley, California 94720-1730

This paper presents a deterministic performance assessment for spent fuel from deep-burn modular high-temperature reactors (DBMHRs) in the proposed Yucca Mountain repository. Typical DBMHR designs utilize fuel elements manufactured from graphite. The fuel itself is made of TRISO particles containing the fissile material. The performance of the DBMHR spent fuel (DBSF) was evaluated in terms of the annual dose to the reasonably maximally exposed individual (RMEI) under various hydrogeological conditions. Part of this evaluation was an analysis of the graphite waste matrix and of the TRISO particles under repository conditions, the result of which indicates that the lifetime of the graphite matrix greatly exceeds that of the TRISO particles and that it is the graphite, not the TRISO particles, that serves to sequester the radionuclides within the fuel matrix. Under all 14 cases considered, DBSF is seen to comply with the annual dose standards set in Part 197 of Title 40 of the Code of Federal Regulations, for exposure via groundwater contamination under current climatic conditions. Parametric studies for the effect of waste matrix lifetime on annual dose received by the RMEI indicate that repository performance is sensitively linked to waste matrix durability because most radionuclides including actinides are likely to be released congruently with the graphite matrix.

I. INTRODUCTION

High-temperature reactors have been proposed to incinerate transuranics (TRUs), including plutonium, americium, and neptunium (and possibly curium) derived from light water reactor spent fuel. This concept is referred to as deep burn because fissioning of TRU elements above 60% of the initial load can be attained in a single pass of the fuel through the reactor.[1] This use of a deep-burn modular high-temperature reactor (DBMHR) to recycle commercial spent nuclear fuel (CSNF) offers remarkable benefits including the extraction of additional electricity, added proliferation resistance, and a reduction of the radiotoxicity of the spent fuel.[1–4] Two central features of the DBMHR are the TRISO fuel particles and the all-graphite core.

Typical DBMHR designs utilize prismatic fuel elements[1] (Fig. 1). These are hexagonal graphite blocks (fuel elements) penetrated by 324 holes arranged in a hexagonal lattice, 216 of which are filled with fuel and 108 of which are used for the coolant flow. The fuel is made of TRISO particles, which contain the fissile material. The TRISO particles are small, multistructural spheres with a kernel of fissile material, 200 μm in diameter, at the center (Fig. 2). The outer layer of the TRISO particle is composed of pyrolytic carbon (PyC), 40 μm in thickness; the next layer, the main structural component of the particle, is made of silicon carbide (SiC) and is 35 μm thick; this is followed by a second 35-μm layer of PyC; and finally surrounding the fuel kernel is a layer of porous carbon 120 μm thick. These particles are dispersed in a graphite matrix that forms cylindrical compacts 4.928 cm long and 1.245 cm in diameter. The compacts are inserted into the fuel channels (3126 compacts per fuel element). The fuel elements, 79.3 cm tall and 36 cm wide flat to flat, are configured in a hexagonal array on multiple levels to form the active region of the core.[2,5] Further design
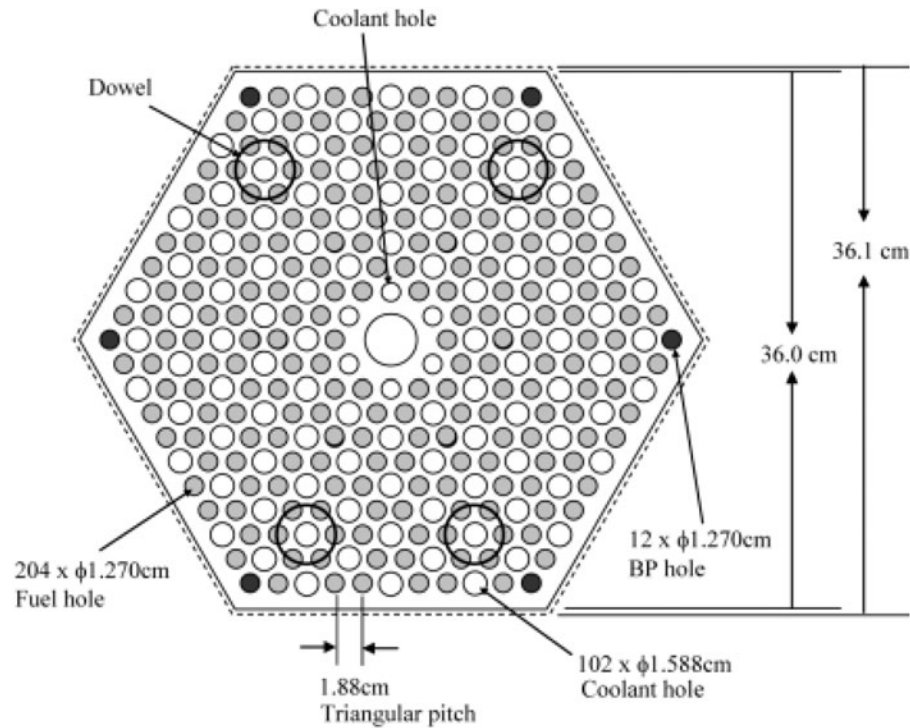
*E-mail: ahn@nuc.berkeley.edu

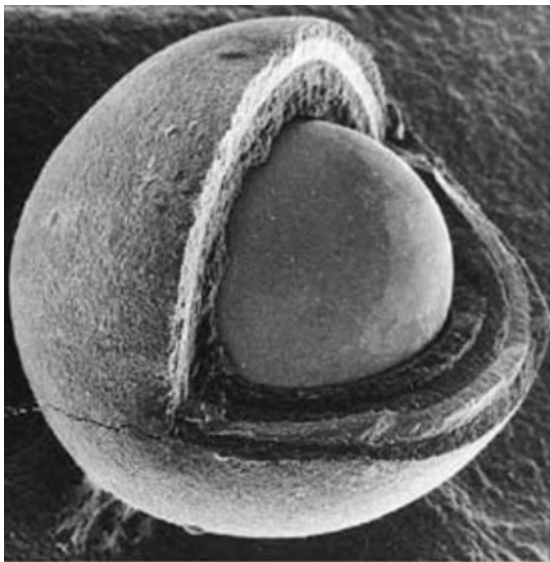Fig. 1. Cross section of hexagonal fuel element.[4]

Fig. 2. Scanning electron microscopy image of TRISO particle showing fuel kernel, porous carbon buffer layer, inner PyC layer, SiC layer, and outer PyC layer.[3]

parameters for the fuel compacts and fuel elements are seen in Table I. This all-graphite core design of the DBMHR is reported to be highly attractive from a repository perspective because of the extremely slow corrosion of graphite in both air and water.[6–8]

The objective of this study is to evaluate the performance of DBMHR spent fuel (DBSF) for final geological disposition. We have chosen the Yucca Mountain geological repository (YMR) as the environment for our study based on the completeness of the data sets necessary to conduct this study and because the regulations associated with the YMR provide a clear basis for evaluating the performance of the spent fuel. In addition, it should be noted that the models used in this study for radionuclide transport in the near and far fields are generic, so that they will allow for a comparison across a wide range of repository environments, given specified performance standards.

An extensive literature review on the geological disposition of DBSF has identified a number of studies in this area. The relevant studies have mainly focused on the performance of the materials that constitute DBSF under repository conditions,[6–8] radiotoxicity assessments of the spent-fuel form,[1,4,5] studies of failure mechanisms and rates for the TRISO particles,[9,10] and DBSF lifetime estimates.[1,8] While these studies are relevant to the repository performance of the spent fuel, they do not constitute a performance assessment of the spent-fuel form, which is to say that no studies have been identified that characterize the release and transport of materials from DBSF stored in a geological repository or the potential health hazard posed to the public from such disposal.

A performance assessment of DBSF can only be made relative to predetermined standards for evaluation.

Fuel Compact and Fuel Element Composition
and Dimensions

TRISO Fuel[1,3]	
Fuel type	TRUO$_{1.7}$
Kernel (diameter, μm/density, g/cm^3)	200/10.0
Buffer layer (thickness, μm/density, g/cm^3)	120/1.05
Inner PyC layer (thickness, μm/density, g/cm^3)	35/1.9
SiC layer (thickness, μm/density, g/cm^3)	35/3.18
Outer PyC layer (thickness, μm/density, g/cm^3)	40/1.9
Isotopic Composition of Fresh TRISO Kernel[5] (wt%)	
^{237}Np	6.8
^{238}Pu	2.9
^{239}Pu	49.5
^{240}Pu	23
^{241}Pu	8.8
^{242}Pu	4.9
^{241}Am	2.8
^{242m}Am	0.02
^{243}Am	1.4
Fuel Compact[1,3]	
Radius (cm)	0.6225
Length (cm)	4.928
Matrix (density, g/cm^3)	1.7
Packing fraction (%)	14
Number of TRISO particles per average compact	5580
Fuel Element[1,3]	
Mass of graphite per element (kg)	90
Dimensions (length, mm/across flats of hexagon, mm)	794/360
Volume (m^3)	0.0889
Number of fuel channels	210
Number of fuel channels under dowels	24
Number of compacts per fuel channel (under dowels/not under dowels)	1/15
Number of compacts per element	3126
Waste Package[3] (MPC)	
Capacity (number of elements)	42
Outside diameter (m)	1.397
Length (m)	5.144

In the case of the YMR, the Environmental Protection Agency issued radiation protection standards for the potential spent nuclear fuel and high-level radioactive waste disposal system in Yucca Mountain, Nevada. These standards are found in Part 197 of Title 40 of the *Code of*

Federal Regulations.[11] The standards are 15 mrem (1.5×10^{-4} Sv) annual committed effective dose equivalent (CEDE) to the reasonably maximally exposed individual (RMEI) for 10 000 yr after repository closure and 100 mrem (1.0×10^{-3} Sv) CEDE to the RMEI for between 10 000 and 1 000 000 yr after repository closure. No regulatory limits are set for times >1 000 000 yr after repository closure. Because there are no subsystem performance requirements,[12] the performance assessment of the DBSF needs to be extended to the point of evaluation of the annual dose to the RMEI.

The main efforts of this study, therefore, are to determine the relevant physical processes and parameters necessary to evaluate the performance of the DBSF in the YMR and to calculate the annual dose delivered to the RMEI as a result of the disposal of DBSF. From this perspective, we divide the performance evaluation for DBSF into two regions: the near field (source term) and the far field (dose evaluation).

The near-field evaluation includes physical models for the processes involving the constituent materials of the DBSF and of other engineered barriers and the diffusive transport of radionuclides released from the DBSF as it degrades. It should be noted that the role of this region is primarily confinement of radioactive materials and that the fidelity of the models in this region can be improved as scientific understanding of the processes improves. In this study, while recognizing this, due to lack of extensive experimental studies, we have applied simplified models. First, the lifetime of the graphite waste form in contact with groundwater is evaluated by a simplification of the geometry of the spent-fuel form. Second, the lifetime of the TRISO particles has been evaluated by a simplified particle-failure model.

The far-field dose evaluation includes models for radionuclide transport in geological formations and for evaluation of annual dose to the RMEI. In contrast to the near-field region, the primary role of this region is dispersion of radioactive materials by hydrological processes in addition to radioactive decay loss during the transport between time of leakage from the near field to time of intake by the RMEI. This part of the evaluation inevitably contains significant, irreducible uncertainties and model hypotheses, particularly for the models in the biosphere. Therefore, for the present investigation, we have decided to use the stylized and abstracted model for radionuclide transport developed in the Department of Nuclear Engineering at the University of California, Berkeley (UC Berkeley), called Transfer to Biosphere,[13] or TTB. With this model, the mass release rates of radionuclides at a point 18 km down gradient from the repository are calculated, consistent with the definition of the RMEI. The annual dose to the RMEI is determined by applying the biosphere model presented in the license application for the YMR (TSPA-LA) for exposure via groundwater contamination under the current climatic conditions.

TABLE II

DBSF Radionuclide Inventory

		Inventory DBSF/Package	
Nuclide	Half-Life (yr)	DBSF at Discharge from DBMHR (mol)	DBSF at Package Failure, 1000 yr (mol)
^{14}C	5.72E+03[a]	1.06E−06	9.35E−07
^{79}Se	2.95E+05	2.55E−02	2.52E−02
^{90}Sr	2.88E+01	1.43E+00	5.05E−11
^{99}Tc	2.13E+05	4.51E+00	4.50E+00
^{126}Sn	2.50E+05	1.11E−01	1.11E−01
^{129}I	1.57E+07	4.08E−02	4.08E−02
^{135}Cs	2.30E+06	2.67E+00	2.67E+00
^{137}Cs	3.01E+01	5.17E+00	5.16E−10
^{210}Pb	2.23E+01	1.12E−13	1.16E−06
^{226}Ra	1.60E+03	3.35E−12	8.43E−05
^{228}Ra	5.76E+00	1.50E−20	5.90E−15
^{227}Ac	2.18E+01	4.88E−13	5.08E−11
^{229}Th	7.30E+03	2.50E−09	3.53E−06
^{230}Th	7.54E+0	3.84E−07	1.85E−02
^{232}Th	1.40E+10	3.54E−10	1.44E−05
^{231}Pa	3.28E+04	4.31E−08	7.88E−08
^{237}Np	2.14E+06	3.17E+00	7.57E+00
^{232}U	6.98E+01	1.80E−06	3.11E−10
^{233}U	1.59E+05	3.45E−06	1.90E−03
^{234}U	2.46E+05	1.09E−01	7.62E+00
^{235}U	7.04E+08	2.15E−02	5.37E−02
^{236}U	2.34E+07	7.88E−03	9.69E−01
^{238}U	4.47E+09	5.60E−01	2.70E−02
^{238}Pu	8.77E+01	7.54E+00	2.93E−02
^{239}Pu	2.41E+04	9.77E−01	1.27E+00
^{240}Pu	6.56E+03	5.52E+00	8.64E+00
^{241}Pu	1.40E+01	5.25E+00	4.18E−04
^{242}Pu	3.75E+05	1.48E+01	1.48E+01
^{241}Am	4.33E+02	2.92E−01	1.15E+00
^{243}Am	7.37E+03	3.39E+00	3.09E+00
^{245}Cm	9.30E+03	2.75E−01	2.53E−01

[a]Read as 5.72×10^3.

Among the 31 important radionuclides listed in Table II, 26 are tracked and transported. The five radionuclides that are not tracked and transported are ^{245}Cm, ^{241}Pu, ^{227}Ac, ^{228}Ra, and ^{210}Pb. In the TSPA-LA, doses from ^{227}Ac, ^{228}Ra, and ^{210}Pb are calculated by assuming they are in secular equilibrium with ^{231}Pa, ^{232}Th, and ^{226}Ra, respectively, because their half-lives are short. Doses from ^{245}Cm and ^{241}Pu are not calculated in the TSPA-LA because they are only important for their decay effects on the inventory of ^{241}Am and ^{237}Np, as stated in Table 7-1 of Ref. 14.

II. NEAR-FIELD CONSIDERATIONS

II.A. DBSF Composition

To begin a discussion about the near-field behavior of DBSF in the YMR, we have evaluated the composition

of the DBSF. As is mentioned above, the DBSF is comprised of hexagonal fuel elements loaded with cylindrical fuel compacts containing the TRISO particles (Fig. 3). It is the TRISO particles that contain the fissile material necessary to generate the heat for operating the DBMHR. The DBMHR fuel and TRISO geometry and physical characteristics are shown in Fig. 2 and Table I.

The radionuclide inventory in the DBSF is determined by the recycling scheme for CSNF. We consider CSNF from a pressurized water reactor (PWR) with a burnup of 50 GWd/tonne U and a 5-yr cooling time. We consider the reprocessing of the CSNF in a UREX-type process with complete removal of U, Cm, and fission products. The Am, Np, and Pu are recovered from the CSNF and fabricated into TRISO fuel. The composition of the fresh DBMHR fuel is shown in Table I. This fresh TRISO fuel is burned one time for 1052 d in a DBMHR to a burnup of 621 GWd/tonne HM (Ref. 5) (Fig. 4).

To evaluate the DBSF composition, a single fuel block with reflective boundary conditions on all sides is considered (Fig. 1). Out of the 216 fuel channels in each fuel element, 6 are modeled as empty because these channels are reserved for burnable poisons (BPs). In this model, however, these poisons are not taken into account.

The depletion analysis was performed assuming a uniform power across the core using MOCUP (MCNP-ORIGEN Coupled Utility Program).[15] MOCUP is a set of scripts that couples MCNP (Ref. 16) and ORIGEN2

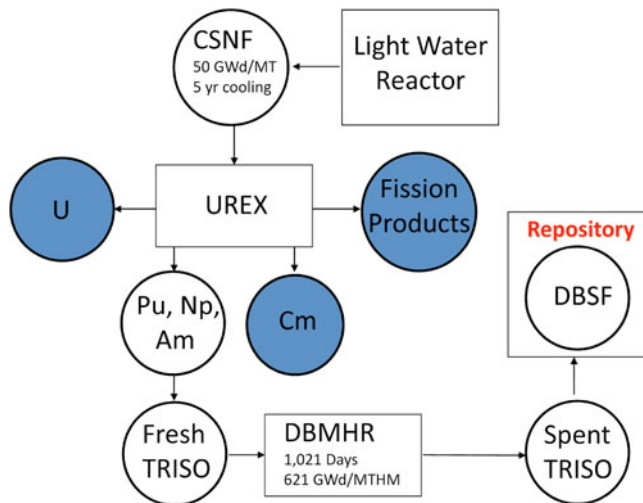Fig. 3. TRISO particles, fuel compacts, and hexagonal fuel element.

Fig. 4. Mass flow diagram for the DBMHR fuel cycle.

TABLE III

Graphite, SiC, and PyC Degradation Rates in Aqueous Solutions*

Material	Aqueous Solution	Atmosphere	R $(g \cdot m^{-2}/d)$
Graphite	Brine	Argon	1.70E−08[a]
Graphite	Water	Oxygen	1.29E−06
Graphite (irradiated)	Brine	Argon	1.28E−05
PyC	Brine	Oxygen	9.30E−08
PyC	Water	Oxygen	4.70E−07
PyC (irradiated)	Brine	Argon	2.60E−05
SiC	Water	Air	2.03E−06
SiC	Brine	Air	4.09E−05

*Reference 7.
[a]Read as 1.70×10^{-8}.

(Ref. 17) to solve time-dependent depletion problems. MCNP provides flux and reaction rates for each of the nuclides to be depleted. These are used to calculate effective one-group cross sections for input in ORIGEN2 along with the initial fuel composition. ORIGEN2 performs the depletion analysis according to the time and power (or flux) provided in the input and outputs the depleted materials composition at the end of the time step. These updated compositions are transferred back to MCNP to determine a new set of cross sections. The process is iterated for as many time steps as required by the user. The MOCUP version in use at UC Berkeley includes a number of improvements added to the original version. In particular an extra script is used to modify the branching ratio of ^{241}Am (n, γ) to ^{242}Am and ^{242m}Am according to the user need, and another script determines the power distributions among the depletion zones using MCNP fission rate tallies.[18] The composition of the DBSF can be seen in Table II.

II.B. Graphite Waste Form Durability

For a discussion about the near-field behavior of DBSF, we need to understand the behavior of the elements that compose the spent-fuel form. In the case of DBSF, the two main components are the graphite matrix and the TRISO particles, each of which serves as an engineered barrier against the release of radionuclides from the spent fuel. We begin our discussion with an assessment of the lifetime of the graphite matrix when in contact with groundwater.

The process of oxidation that takes place when graphite comes into contact with liquid water in the presence of air occurs with the dissolved oxygen in the water and with oxygen absorbed on the surface of the graphite, not with the water itself, although the water catalyzes the

reaction.[7] This is evidenced by the fact that the oxidation rate is higher in the presence of water and the activation energy is lower.[7] Further, degradation studies performed on graphite in various aqueous solutions revealed the absence of hydrogen or carbon monoxide in the gas-phase composition, which indicates that corrosion is not caused by the interaction of graphite with water.[7,19] Table III provides graphite corrosion rates in a number of aqueous solutions and under various gaseous atmospheres.

For the oxidation of the graphite waste matrix, we make the following simplifying assumptions. We first make a geometric transformation of the DBSF from 42 hexagonal fuel elements (in the case of whole-element disposal), or a single cylindrical fuel compact (in the case of compact-only disposal), into a graphite sphere of equivalent mass. Additionally, we consider that the rate at which the oxidation proceeds remains constant. If we consider a sphere of radius r (in m) and density ρ (in kg/m^3) degrading at a rate R (in kg$\cdot$m^{-2}/s), then the rate of change of the radius of the sphere is given as

$$\frac{dr}{dt} = \frac{R}{\rho} \ , \tag{1}$$

and the time it takes to completely degrade the sphere is given as

$$t = \frac{r_0 \rho}{R} \ , \tag{2}$$

where r_0 is the initial radius of the sphere. Using this formulation we can make a calculation of the lifetime of the graphite waste matrix of the DBSF.

Figure 5 shows the proposed multipurpose canister (MPC) for the disposal of DBSF in the YMR. Each MPC can contain 42 fuel elements. In considering the lifetime of the DBSF, we consider four disposal scenarios: (a) whole-element disposal and (b) compact-only
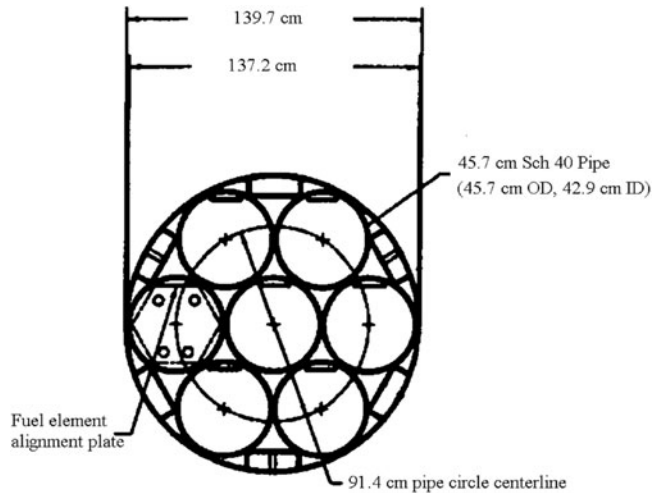
Fig. 5. MPC and waste loading.[1]

disposal, each in the fast and slow limits of graphite oxidation.

The whole-element disposal scenario considers the disposal of 42 fuel elements per MPC; the geometric transformation to a spherical form is made by considering that the entire mass of graphite in the MPC is converted into a monolithic sphere. In the compact-only disposal scenario, we consider that the unit of waste that is being degraded is the single fuel compact. We consider that these four cases will represent the bounding values for the lifetime of the graphite waste matrix in the MPC after it has breached.

Figure 6 shows the fractional amounts of graphite remaining in a failed waste package as a function of time
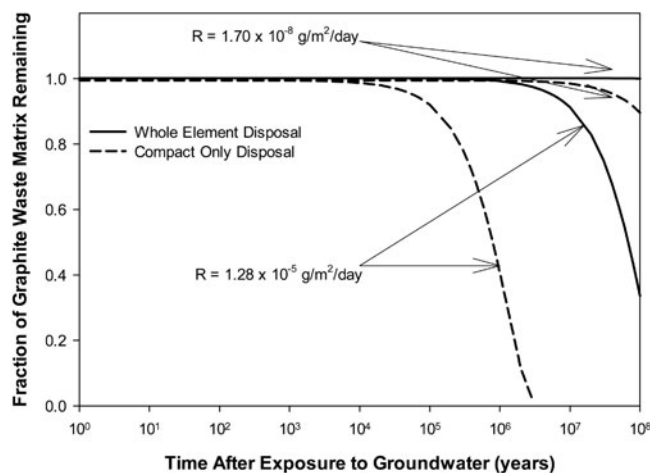

Fig. 6. Fractional amount of waste matrix remaining in MPC after canister failure.

after groundwater contact. As can be seen from Fig. 6, the worst case among the four cases, i.e., the compact-only disposal (the smallest total graphite mass) coupled with the fast oxidation regime, produces a matrix lifetime of >3 million yr. If we consider the scenario of the whole-element disposal in the fast oxidation regime, the matrix lifetime is $>3 \times 10^8$ yr. This long lifetime hints at the possible use of graphite as a highly durable waste form for the disposal of high-level waste, especially under oxidizing conditions, as is the case in the YMR. In light of this robust performance of the waste matrix, it remains to be seen if the TRISO layers significantly contribute as an engineered barrier against the release of radionuclides from the spent-fuel form.

II.C. TRISO Particle Failure Model

When considering the performance of DBSF in a geological repository as a waste form, we must also consider the behavior of the TRISO particles. Central to the performance of the TRISO particles is the performance of the SiC layer, which is the TRISO particle's main structural component. The layers of the TRISO particle act as a pressure vessel, containing the remaining actinide elements and fission products, some of which are gases.[1–3,9] Helium gas generated from alpha decay[1,3] of actinide isotopes will also build up in the TRISO particle while in the repository. Thus, the pressure in the spent TRISO particle is due to the fission gases generated in a reactor and the helium gas from alpha decay while in the repository.

When the tensile stresses in the SiC layer exceed its strength, the SiC layer ruptures, and the TRISO particle is considered to have failed. It has been reported[1,3] that the stress in the SiC layer due to gases within the particle is given by

$$\sigma(t) = \frac{p(t)R_{\text{SiC}}}{2x_{\text{SiC}}(t)} \ , \qquad (3)$$

where

$p(t)$ = time-dependent internal pressure in the TRISO particle due to fission gases and helium from alpha decay at time t

R_{SiC} = radius to the middle of the SiC layer

$x_{\text{SiC}}(t)$ = thickness of the SiC layer at time t.

The probability of failure of the particle can be expressed as a Weibull distribution,[1,3]

$$P_f(t) = 1 - \exp\left[-\ln 2 \times \left(\frac{\sigma(t)}{\sigma_f}\right)^M\right] \ , \qquad (4)$$

where

$P_f(t)$ = cumulative probability of failure at time t

$\sigma(t)$ = hoop stress in the SiC layer at time t

σ_f = mean fracture strength of the SiC layer

M = Weibull parameter.

In our evaluation of the lifetime, σ_f is assigned the value of 388 MPa and M is set to 7.9 (Refs. 3 and 20). The volume available to gases was calculated from the dimensions of the TRISO particle given in Table I by considering that the void fraction of the porous buffer layer is 0.5, that the void fraction of the fuel kernel is 0.07, and that the inner PyC layer forms the boundary of the available volume.[10]

Figure 7 shows the relation of the internal pressure in the TRISO particle to the time after discharge from the reactor. The internal pressure is calculated using the ideal gas law at 25°C and by assuming that the only contributors to the pressure are the noble gases generated during burnup and the helium accumulated after discharge by radioactive decay of alpha-emitting nuclides. These time-dependent concentrations were calculated by the ORIGEN2 code. By assuming a kernel temperature of 25°C, we have effectively neglected the heat resulting from the decay of the short-lived fission products. In our model this will lead to a lower internal pressure, which will in turn result in a longer overall lifetime for the SiC layer. Effects of assuming a low temperature will be discussed below in this section where model simplification is discussed.

After emplacement in the repository, the failure of the TRISO fuel particle is considered to occur during the degradation of the DBSF due to exposure to groundwater. As the outer PyC layer is eroded by contact with groundwater, the SiC layer will be exposed and will subsequently erode. Experimental data are available for the dissolution rates of graphite, SiC, and PyC in several different aqueous solutions and at a number of temperatures. The data are summarized in Table III.

We can formulate the time-dependent thickness of the SiC layer as

$$x_{\mathrm{SiC}}(t) = r_{\mathrm{SiCo}} - r_{\mathrm{SiCi}} - \frac{Rt}{\rho} \ , \qquad (5)$$

where

ρ = density of the SiC layer

R = corrosion rate $(\mathrm{g \cdot m^{-2}/yr})$

r_{SiCo} = initial outer radius of the SiC layer

r_{SiCi} = radius of the inner surface of the SiC layer.

A calculation of the lifetime of the SiC layer exposed to water corrosion can be made if we make use of Eq. (5), the internal pressure data presented in Fig. 7, and the failure models presented above in Eqs. (3) and (4). Substituting Eq. (5) into Eq. (3) yields

$$\sigma(t) = \frac{p(t) R_{\mathrm{SiC}}}{2\left(r_{\mathrm{SiCo}} - r_{\mathrm{SiCi}} - \dfrac{Rt}{\rho}\right)} \ , \qquad (6)$$

which upon substitution into Eq. (4) results in the formula for the overall probability of failure of the SiC layer in the form of

$$P_f = 1 - \exp\left[-\ln 2 \times \left(\frac{\dfrac{p(t) R_{\mathrm{SiC}}}{2\left(r_{\mathrm{SiCo}} - r_{\mathrm{SiCi}} - \dfrac{Rt}{\rho}\right)}}{\sigma_f} \right)^M \right] .$$

$$(7)$$

The corrosion rates R for the SiC layer are taken to be the high and low rates of corrosion presented in Table III. The material properties and dimensions of the TRISO particle and the SiC layer are given in Table I.

Figure 8 shows that the effective lifetime of the SiC layer is sensitively dependent on the corrosion rate and the model used to predict the stress in the SiC layer. The two curves shown in Fig. 8 represent the bounding cases for the cumulative failure probability given the available experimental data. We can see that the SiC layers have a lifetime (time to total failure) of between 7000 and 140 000 yr (neglecting the protective effects of the outer PyC layer). If we include the protective effects of the outer PyC layer by considering a similar dissolution model as given by Eq. (1), then the lifetime of the TRISO particle is extended to up to a maximum lifetime of 2 million yr. This is seen to be much less than the calculated
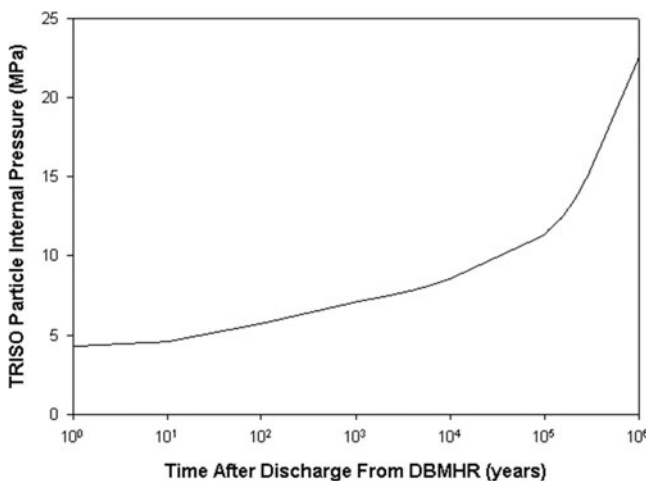

Fig. 7. TRISO particle internal pressure as a function of time after discharge from the reactor.
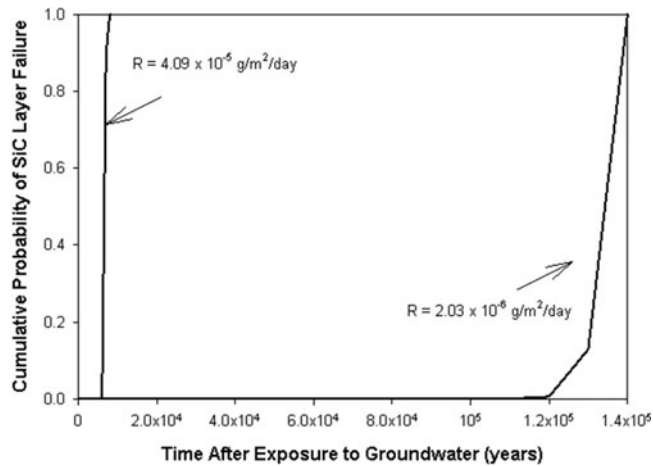
Fig. 8. Cumulative probability of SiC layer failure as a function of time exposed to groundwater.

lifetime of the graphite waste matrix (3×10^6 to 3×10^8 yr in the fast graphite oxidation regime).

Because of this significant difference between the lifetimes of graphite and the TRISO particle and because of the large number of TRISO particles embedded in the graphite matrix, in the remainder of our discussion, we assume that the TRISO layers do not serve as a barrier that delays the release of radionuclides from failed waste packages and that the radionuclides in the TRISO particle are homogeneously dispersed in the graphite matrix. Thus, the radionuclides are assumed to be released by degradation of the graphite matrix. Note that for the TRISO particle lifetime the temperature of 25°C has been assumed, which resulted in overestimation of the particle lifetime. Thus, if we take into account elevated kernel temperatures, or additional gases, this simplification assumption would still be further supported.

II.D. Disposal Timeline and Drift Shadow Description

In the proposed YMR, the DBSF will be loaded into MPCs and placed into tunnel drifts.[1,3] In the early years after repository closure, the tunnel walls will heat up and dry out from heat generated from the decay of short-lived fission products.[21] After these fission products have decayed away, the temperature in the drift walls will fall, and water will reinfiltrate the pores of the rock that comprises the drift wall. Subsequently, water will begin to infiltrate the drift tunnel and will contact the MPC (neglecting the drip shield). After package failure, water will be able to enter the MPC and will begin degrading the graphite waste matrix and TRISO particles, and eventually the water will begin to dissolve the radionuclides within the MPC. This water, laden with radionuclides, will then exit the MPC and will enter the near-field host rock.

The host rock in the region immediately below the tunnel drift is called the drift shadow region.[22–24] The drift shadow is a region in the unsaturated zone beneath the tunnel drift that is partially sheltered from downward-percolating water, because the capillary action is not strong enough to draw water into the rock immediately below the drift (Fig. 9). Transport in this region is controlled mainly by diffusive processes, rather than by advection.[22–24] The radiocuclides will diffuse through this region until they reach a location at which they can be transported by advection through the fracture network in the unsaturated zone to the alluvium, at which point they will travel by advection to some down-gradient location. The shortest diffusion path to a region of advective transport will be to consider that the contaminated water is released from an outside edge of the waste canister and is subsequently diffusively transported laterally to the edge of the tunnel drift (or equivalently to the edge of the drift shadow region), a distance somewhat >2 m. In the remainder of the analysis, we consider that the length of diffusive transport in the near field is 2 m.
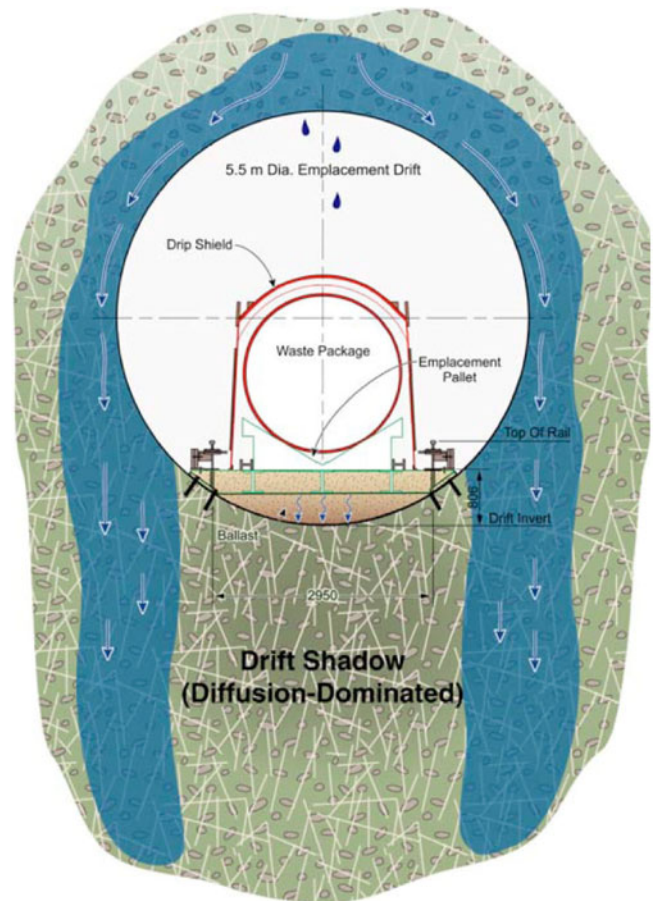

Fig. 9. Drift shadow concept.[24]

II.E. Near-Field Model

For our analysis, we consider a geometric transformation of the DBSF. In the case of the whole-element disposal, we consider the transformation of 42 fuel elements into a single sphere of equivalent mass. In the case of the compact-only disposal, we consider the transformation of a single fuel compact into a sphere of equivalent mass. Figure 10 shows the geometry of the near-field region. Recalling that the lifetime of the TRISO layers is seen to be substantially less than that of the graphite waste matrix, we consider that the TRISO layers do not serve as an engineered barrier against the release of radionuclides from the surface of the DBSF, and that the radionuclide inventory is distributed homogeneously throughout the graphite waste matrix, rather than discreetly in TRISO particles. The graphite sphere is then considered to be surrounded by a diffusion barrier whose thickness is 2 m. This diffusion barrier is considered to be host rock in the drift shadow region. Although there are a number of different rock types in the proposed YMR, the current repository design locates ~70% of the drifts in the tsw35 hydrogeologic unit.[23,25] The supporting documentation for the TSPA-LA provides distributions for the essential physical parameters necessary to make the near-field calculations.

When the graphite matrix comes into contact with groundwater, the matrix begins to dissolve and radionuclides are released. The release of radionuclides can be considered to occur by two modes in this model: congruent release and solubility-limited release.[13] In the case of congruent release, the fractional release rate of the nuclide is equal to the fractional dissolution rate of the waste matrix, or graphite. If the solubility of an individual radionuclide is low, then a precipitate of the nuclide will form. The precipitate slowly dissolves at a rate given by the rate of mass transfer into the water in the pores in the surrounding medium, with the concentration of the nuclide in the water adjacent to the surface of the waste form given by its solubility. Note that the radionuclide
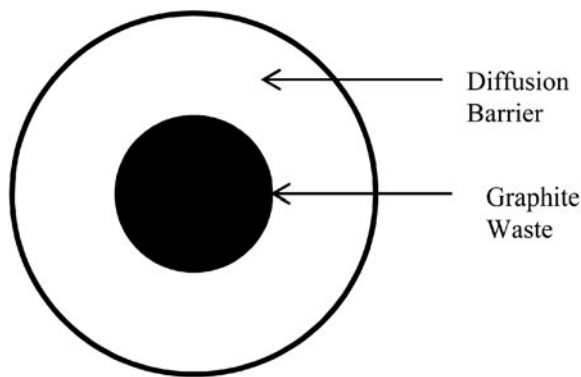
release mode is determined not only by its solubility, but also by the rate of matrix dissolution, the radionuclide inventory in the waste form, and the rate of diffusive mass transfer at the point of matrix dissolution. The TTB code can determine the release mode by considering the material balance of each nuclide.[13] For the case of a graphite waste matrix, the oxidation rates of the graphite are taken to be the fast and slow limits of graphite oxidation provided in Table III. The mathematical formulation for the release rate of radionuclides from the surface of the DBSF can be found in Ref. 13.

A number of assumptions were made to obtain a conservative (over)estimate of the concentration of radionuclides in the diffusion barrier region released from the graphite waste form as it degrades. We give no protective credit to the drip shield, or to the MPC, and we assume that canister failure occurs simultaneously at 1000 yr. Because this is a deterministic assessment of the performance of DBSF relative to Ref. 11, we have chosen 1000 yr as the package failure time in order to have a dose to evaluate with respect to the regulatory dose limits in the first 10 000 yr. In actuality, <1% of all packages are expected to fail in the first 1000 yr (Ref. 21). All radionuclide releases are considered in the maximum limit of their solubility.

II.F. Mathematical Formulation for Near-Field Transport

As outlined above, we consider the geometric transformation of the DBSF into a sphere surrounded by a concentric spherical diffusion barrier. We will consider that the following physical mechanisms will be sufficient to describe the transport of radionuclides within the diffusion barrier region: sorption with the host rock, radioactive decay, and diffusive transport. Given these physical mechanisms, the concentration of radionuclides in the water phase of the diffusion barrier will be given by

$$K_{e(1)} \frac{\partial N_1}{\partial t} + \lambda_1 K_{e(1)} N_1 = D_{e(1)} \frac{1}{r^2} \frac{\partial}{\partial r} \left(r^2 \frac{\partial N_1}{\partial t} \right) ,$$

$$K_{e(2)} \frac{\partial N_2}{\partial t} + \lambda_2 K_{e(2)} N_2 = D_{e(2)} \frac{1}{r^2} \frac{\partial}{\partial r} \left(r^2 \frac{\partial N_2}{\partial t} \right)$$
$$+ \lambda_1 K_{e(1)} N_1 ,$$

$$\vdots \qquad \vdots \qquad \vdots$$

$$K_{e(i)} \frac{\partial N_i}{\partial t} + \lambda_i K_{e(i)} N_i = D_{e(i)} \frac{1}{r^2} \frac{\partial}{\partial r} \left(r^2 \frac{\partial N_i}{\partial t} \right)$$
$$+ \lambda_{i-1} K_{e(i-1)} N_{i-1} ,$$

$$t > 0, \, r_1 < r < r_2, \, i = 1, 2, \ldots, I \ , \qquad (8)$$

Fig. 10. Geometry in the near field showing spherical waste form and surrounding diffusion barrier.

where

$N_k(r, t)$ = concentration of the k'th member radionuclide in a decay chain of length I (mol/m^3)

r = distance from the center of the waste form (m)

$K_{e(k)}$ = retardation coefficient for element e

λ_k = decay constant of radionuclide k (yr^{-1}).

The retardation coefficient $K_{e(k)}$ is given as

$$K_{e(k)} = 1 + \frac{\rho(1 + \varepsilon)}{\varepsilon} K_d^e \ , \qquad (9)$$

where ε and ρ (kg/m^3) are the porosity and density, respectively, of the drift shadow region and K_d^e (m^3/kg) is the equilibrium sorption distribution coefficient for element e in the diffusion barrier. The solution of these governing equations provides the concentration of radionuclides in the diffusion barrier region. We can also determine the mass flux of radionuclides across the outer boundary of the diffusion barrier. This mass flux will be used as a source term for the input of radionuclides in our far-field transport calculations. A detailed solution of the governing equations is provided in Ref. 13.

III. FAR-FIELD CONSIDERATIONS

III.A. Far-Field Model and Physical Processes

The drifts in the YMR are situated some 300 m below the ground surface and ~300 m above the water table. Once radionuclides have been released from the waste packages, they must traverse the unsaturated zone to reach the saturated zone where they can be transported down gradient through a network of fractures to the alluvium and subsequently to the RMEI, located a total distance of 18 km down gradient from the repository. Transport of radionuclides in the saturated zone occurs, then, in two regions. In the first 15 km down gradient from the repository, transport occurs via advection in the fractures of fractured volcanic rock. At the 15-km location, the radionuclides enter the alluvial zone, where transport takes place as advection through a porous medium for the next 3 km (Ref. 21). Transport time is significantly shorter through the fracture network than in the alluvium[21]; therefore, we consider transport to the 18-km location to occur exclusively in the fractured volcanic rock.

The unsaturated zone is composed of a number of different rock types with varying physical properties.[26,27] The transport of radionuclides to the saturated zone occurs mainly by advection through fractures permeating the unsaturated host rock (although also by diffusion through the rock matrix); however, a number of major faults intersect the unsaturated host rock and act as a fast path from the tunnel drifts to the saturated zone.[21,26,27] To simplify our model, in all cases we consider instantaneous transport of radionuclides from the outer edge of the diffusion barrier in the unsaturated zone through these major faults to the saturated zone. With the exception of the narrow diffusion barrier, we neglect the role of the unsaturated zone in slowing the transport of radionuclides into the saturated zone.

The geometry of the far-field transport model is shown in Fig. 11. For transport beyond the diffusion barrier, a fractured volcanic rock matrix with multiple parallel planar fractures is considered. The following physical processes are taken into account: advection in the fractures, longitudinal dispersion, molecular diffusion, sorption, and radioactive decay. The velocity of the water in the fracture and the longitudinal dispersion are considered to be constant and uniform. Additionally, we assume that the permeability of the rock matrix is low enough that transport within the host rock is primarily by molecular diffusion while transport along the fracture is much faster than transport in the rock.

Finally, the annual dose to the RMEI is calculated by evaluating Eq. (10), taken from Ref. 28 for exposure via contaminated groundwater:
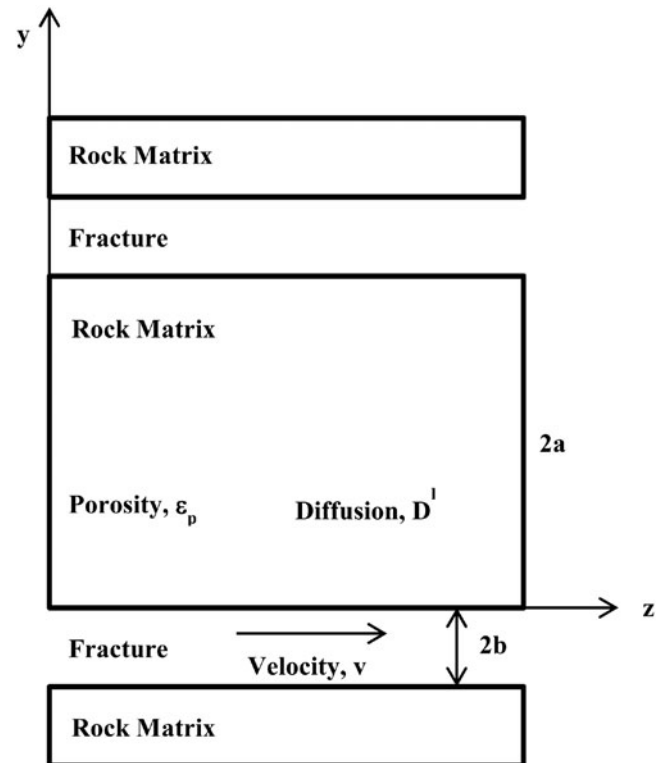

Fig. 11. Far-field transport geometry showing one-dimensional planar fractures and transport mechanisms.

$$D_T(t) = \sum_{j=1}^{N} \mathrm{BDCF}_j \cdot C_j(18 \text{ km}, t) \ , \qquad (10)$$

where

$D_T(t)$ = total time-dependent dose to the RMEI from the N transported radionuclides to the 18-km observation location at time t (Sv/yr).

BDCF_j = biosphere dose conversion factor (BDCF) for radionuclide j (Sv/yr per Bq/m^3)

$C_j(18 \text{ km}, t)$ = time-dependent concentration of radionuclides in the groundwater at the 18-km boundary (Bq/m^3).

The BDCF is a means of translating concentration of radionuclides in the groundwater at the observation location into an annual dose received by the RMEI for the exposure pathway through groundwater transport to the observation point. The BDCF for each radionuclide is determined by considering that the RMEI meets a number of criteria, among which are that they drink 2 ℓ of contaminated water per day and use contaminated well water at a rate of 3000 acre·ft/yr (3.7×10^6 m^3/yr) for various domestic and agricultural purposes. Therefore, the BDCF considers not only direct exposure from the consumption of contaminated groundwater, but also the consumption of contaminated foodstuffs (animals and crops grown with the contaminated water) and other exposure pathways (e.g., inhalation, accidental ingestion of contaminated soil, etc.) associated with the use of contaminated water. Because the BDCF is dependent on a number of factors, it is given in the TSPA-LA as a distribution for three distinct climatic conditions. In our study we assume the mean value of the BDCF for each radionuclide in the current climatic conditions. These values are given in Table IV.

It is assumed that the entire inventory of Pu, Np, and Am included in 63 000 tonnes of CSNF destined for the YMR is converted into fresh DBMHR fuel. Of the CSNF destined for the YMR, 40 200 tonnes are from PWRs and 22 800 tonnes are from boiling water reactors[29] (BWRs). The radionuclide inventories for the representative PWR and BWR spent fuel assemblies are listed, respectively, in Tables A-12 and A-13 of Ref. 30. The total number of DBSF waste packages is calculated to be 23 612 from this inventory; this is based on the complete utilization of the ^{239}Pu inventory in the 63 000 tonnes of CSNF. The transport calculations for the whole-element disposal are obtained by considering a single waste package. The annual dose to the RMEI in this case is scaled by the total number of packages. The transport calculations for the compact-only disposal are made by considering the degradation of a single fuel compact, and the annual dose to the RMEI is obtained by scaling the dose by the total number of compacts destined for the YMR (23 612 packages $\times$ 3126 compacts per fuel element $\times$ 42 fuel elements per package).

III.B. Mathematical Formulation for Far-Field Transport

With these assumptions, the equations governing the concentration of radionuclides in the fracture $C_k(z,t)$ and in the pores $C_k^p(y,t;z)$ are

TABLE IV

Bisophere Dose Conversion Factors*

Nuclide	BDCF (Sv/yr per Bq/m^3)	Nuclide	BDCF (Sv/yr per Bq/m^3)	Nuclide	BDCF (Sv/yr per Bq/m^3)
^{14}C	1.93E−09[a]	^{227}Ac	1.30E−06	^{238}U	7.87E−08
^{79}Se	2.42E−08	^{228}Th	3.15E−07	^{237}Np	2.74E−07
^{90}Sr	3.43E−08	^{229}Th	2.58E−06	^{238}Pu	7.61E−07
^{99}Tc	1.12E−09	^{230}Th	1.08E−06	^{239}Pu	9.55E−07
^{126}Sn	4.33E−07	^{232}Th	1.85E−06	^{240}Pu	9.51E−07
^{129}I	1.29E−07	^{231}Pa	2.44E−06	^{242}Pu	9.07E−07
^{135}Cs	1.45E−08	^{232}U	6.04E−07	^{241}Am	8.34E−07
^{137}Cs	1.30E−07	^{233}U	8.97E−08	^{243}Am	8.88E−07
^{210}Pb	2.74E−06	^{234}U	8.19E−08		
^{226}Ra	3.78E−06	^{235}U	9.41E−08		
^{228}Ra	9.05E−07	^{236}U	7.67E−08		

*Reference 37.
[a]Read as 1.93×10^{-9}.

$$R_{e(k)} \frac{\partial C_k}{\partial t} + v \frac{\partial C_k}{\partial z} - D^L \frac{\partial^2 C_k}{\partial^2 z} - \frac{D^I_{e(k)}}{b} \frac{\partial C_k^P}{\partial y}\bigg|_{y=0}$$

$$+ R_{e(k)} \lambda_k C_k - R_{e(k-1)} \lambda_{k-1} C_{k-1} = 0$$

$$t > 0, z > 0 \qquad (11)$$

and

$$\alpha_{e(k)} \frac{\partial C_k^P}{\partial t} = D^I_{e(k)} \frac{\partial^2 C_K^P}{\partial y^2} - \alpha_{e(k)} \lambda_k C_k^P$$

$$+ \alpha_{e(k-1)} \lambda_{k-1} C_{k-1}^P$$

$$t > 0, 0 < y < a, z > 0 \ . \qquad (12)$$

The initial and boundary conditions are given as

$$C_k(z,0) = 0, z > 0 \ ; \qquad (13)$$

$$C_k^P(y,0;z) = 0, 0 < y < a, z > 0 \ ; \qquad (14)$$

$$\varepsilon_f \left[v C_k(0,t) - D^L \frac{\partial C_k}{\partial z}\bigg|_{z=0} \right] = \frac{Q_k(t)}{A} \ , \quad t > 0 \ ;$$

$$(15)$$

$$C_k(\infty, t) = 0 \ , \quad t > 0 \ ; \qquad (16)$$

$$C_k^P(0,t;z) = C_k(z,t) \ , \quad t > 0, z > 0 \ ; \qquad (17)$$

and

$$\frac{\partial C_K^P}{\partial y}\bigg|_{y=0} = 0 \ , \quad t > 0, z > 0 \ . \qquad (18)$$

The time-dependent quantity $Q_k(t)$ is the flux of radionuclide k from the diffusion barrier, and the dimensionless factor A is determined by repository configuration. The Laplace-transformed analytical solutions are presented in Ref. 13 and are inverted numerically to obtain the concentrations at a given distance from the used fuel. For a detailed discussion, see Ref. 13.

The capacity factor for the radionuclide k of element e is given as

$$\alpha_{e(k)} = \varepsilon_p + \rho_p(1 - \varepsilon_p)K_{dp}^e \ , \qquad (19)$$

where ρ_p is the density of the host rock and K_{dp}^e is the sorption distribution coefficient of element e for the host rock. The retardation coefficient $R_{e(k)}$ is given as

$$R_{e(k)} = 1 + \frac{\rho_f(1 - \varepsilon_f)K_{df}^e}{\varepsilon_f} \ , \qquad (20)$$

where

ρ_f = density of the material filling the fractures

ε_f = porosity of the material filling the fractures

K_{df}^e = sorption distribution coefficient of element e for the material filling the fractures.

With this information we are able to solve for the annual dose to the RMEI at the down-gradient observation location.

IV. INPUT PARAMETERS

Tables V, VI, and VII describe the input parameters necessary to perform the calculations for the mathematical models described previously.

IV.A. Transport Parameters

In this study, we have considered (a) optimistic, (b) nominal, and (c) pessimistic cases. These cases were created by varying the hydrogeological parameters associated with radionuclide transport.

The solubilities for radionuclides in the near field were calculated using the PHREEQC geochemical modeling software[31] by considering the YMR nominal environmental conditions and by considering that the graphite in contact with the groundwater will alter the geochemistry of the groundwater.[32] When graphite is exposed to groundwater, the graphite will react with oxygen dissolved in the water. The corrosion product, carbon dioxide, has an important effect on the solubilities of many radionuclides.[33,34] A detailed discussion of the solubility calculations can be found in Refs. 32 and 33. The solubilities of all of the radionuclides are fixed at the highest values for this environment. The equilibrium sorption coefficients are chosen to be their mean values for the respective host rocks, and the matrix diffusion coefficient in the fractured volcanic rock is chosen to be its mean value, as given in the supporting documentation for the TSPA-LA (Refs. 35 and 36).

The water velocity v and longitudinal hydrodynamic dispersion coefficient D_L are assumed to be constant with time and uniform throughout space. They are also assumed to be the same for all nuclides considered because dispersion is mainly determined by the geometry of the transport path.[13] The values for the water velocity were chosen in accordance with measurements made for the TSPA-LA for the YMR in the fractured volcanic rock in the saturated zone. The mean value for the longitudinal dispersion coefficient α_L was chosen, and it is assumed that D_L is given as

$$D_L = \alpha_L v \ . \qquad (21)$$

TABLE V

Assumed Parameters for Use in Optimistic, Nominal, and Pessimistic Transport Calculations

	Optimistic Case	Nominal Case	Pessimistic Case
Waste matrix [1–3,5]	Graphite	Graphite	Graphite
Porosity of the diffusion barrier region, ε (Ref. 37)	0.043	0.12	0.229
Density of the diffusion barrier region, ρ (Ref. 36)	2210	2068	1980
Porosity of the fractured volcanic rock, ε_p (Ref. 36)	0.15	0.20	0.25
Density of the fractured volcanic rock, ρ_p (kg/m^3) (Ref. 36)	2770	1880	1770
Water velocity in the fractures, v (m/yr) (Ref. 36)	0.312	2.37	7.50
Longitudinal dispersion coefficient, D^L (Ref. 36)	0.312	2.37	7.50
Tortuosity correction factor for the diffusion barrier, τ	1	1	1
Fracture hydraulic aperture, $2b$ (m)	2.71E−03[a]	1.97E−02	1.45E−01
Graphite waste form oxidation rate, R (fast oxidation/ slow oxidation) (g·m^{-2}/d) (Ref. 7)	1.28E−05/1.70E−08	1.28E−05/1.70E−08	1.28E−05/1.70E−08
Mass of graphite being degraded (whole-element/ compact-only disposal) (g) (Refs. 1 and 5)	4.93E+06/8.77E+00	4.93E+06/8.77E+00	4.93E+06/8.77E+00
Radius of the equivalent spherical waste, r_1 (whole element/compact only) (m)	0.905/0.011	0.905/0.011	0.905/0.011
Radius of the equivalent spherical diffusion barrier region, r_2 (whole element/compact only) (m)	2.905/2.011	2.905/2.011	2.905/2.011
Surface area of the waste form, $S_1 = 4\pi r_1^2$ (whole element/compact only) (m^2)	10.29/0.0015	10.29/0.0015	10.29/0.0015
Surface area of the diffusion barrier region, $S_2 = 4\pi r_2^2$ (whole element/compact only) (m^2)	106.1/50.82	106.1/50.82	106.1/50.82
Distance between two waste forms (m) (Ref. 1)	5.24	5.24	5.24
Characteristic repository length, L_r (m) (Refs. 1 and 20)	20.6	20.6	20.6
Flowing interval spacing (m) (Ref. 36)	2.71	19.65	145.08
Flowing interval porosity, ε_f (Ref. 36)	1.00E−03	1.00E−03	1.00E−03

[a]Read as 2.71×10^{-3}.

TABLE VI

Assumed Elemental Parameters for Use in Transport Calculation

Element	Solubility N_e (mol/m^3) (Refs. 31 and 32)	Free Water Diffusion Coefficient D_e (m^2/yr) (Ref. 34)	In the Diffusion Barrier K_d^e (m^3/kg) (Ref. 21)	In the Fractured Volcanic Rock K_{dp}^e (m^3/kg) (Ref. 34)	In the Fractured Volcanic Rock D_e^I (m^2/yr) (Ref. 34)
Americium	8.88E+02[a]	1.20E−02	4.00E−01	5.50E+00	1.58E−03
Plutonium	4.23E+02	4.10E−02	1.00E−01	1.00E−01	1.58E−03
Uranium	9.69E+01	2.03E−02	2.00E−04	1.20E−02	1.58E−03
Neptunium	1.65E+02	1.95E−02	1.00E−03	2.88E−03	1.58E−03
Thorium	2.61E+01	1.88E−02	5.50E+00	5.50E+00	1.58E−03
Protactinium	1.65E+01	1.90E−02	5.50E+00	5.50E+00	1.58E−03
Radium	3.09E+02	3.30E−02	3.25E−01	5.50E−01	1.58E−03
Technetium	—	6.14E−02	0.00E+00	0.00E+00	1.58E−03
Carbon	—	3.72E−02	0.00E+00	0.00E+00	1.58E−03
Strontium	—	3.00E−02	2.50E−02	2.10E−01	1.58E−03
Selenium	—	3.26E−02	8.60E−03	1.40E−02	1.58E−03
Tin	5.01E−05	4.88E−02	7.10E−01	1.90E+00	1.58E−03
Iodine	—	6.45E−02	0.00E+00	0.00E+00	1.58E−03
Cesium	—	6.49E−02	2.00E−03	7.28E−01	1.58E−03

[a]Read as 8.88×10^2.

TABLE VII

Retardation Factors for the Diffusion Barrier, Fractured Volcanic Rock, and Fracture

Element	In the Diffusion Barrier K_e			In the Fractured Volcanic Rock a_e			In the Fracture R_e
	Optimistic	Nominal	Pessimistic	Optimistic	Nominal	Pessimistic	All Cases
Americium	$1.97E+04$[a]	$6.07E+03$	$2.67E+03$	$1.30E+04$	$8.27E+03$	$7.30E+03$	$1.00E+00$
Plutonium	$4.92E+03$	$1.52E+03$	$6.68E+02$	$2.36E+02$	$1.50E+02$	$1.33E+02$	$1.00E+00$
Uranium	$1.08E+01$	$4.03E+00$	$2.33E+00$	$2.83E+01$	$1.82E+01$	$1.59E+01$	$1.00E+00$
Neptunium	$5.01E+01$	$1.61E+01$	$7.66E+00$	$6.78E+00$	$4.53E+00$	$3.82E+00$	$1.00E+00$
Thorium	$2.71E+05$	$8.34E+04$	$3.67E+04$	$1.30E+04$	$8.27E+03$	$7.30E+03$	$1.00E+00$
Protactinium	$2.71E+05$	$8.34E+04$	$3.67E+04$	$1.30E+04$	$8.27E+03$	$7.30E+03$	$1.00E+00$
Radium	$1.60E+04$	$4.93E+03$	$2.17E+03$	$1.30E+03$	$8.27E+02$	$7.30E+02$	$1.00E+00$
Technetium	$1.00E+00$	$1.00E+00$	$1.00E+00$	$1.50E-01$	$2.00E-01$	$2.50E-01$	$1.00E+00$
Carbon	$1.00E+00$	$1.00E+00$	$1.00E+00$	$1.50E-01$	$2.00E-01$	$2.50E-01$	$1.00E+00$
Strontium	$1.23E+03$	$3.80E+02$	$1.68E+02$	$4.94E+02$	$3.16E+02$	$2.79E+02$	$1.00E+00$
Selenium	$4.23E+02$	$1.31E+02$	$5.83E+01$	$3.31E+01$	$2.13E+01$	$1.86E+01$	$1.00E+00$
Tin	$3.49E+04$	$1.08E+04$	$4.73E+03$	$4.47E+03$	$2.86E+03$	$2.52E+03$	$1.00E+00$
Iodine	$1.00E+00$	$1.00E+00$	$1.00E+00$	$1.50E-01$	$2.00E-01$	$2.50E-01$	$1.00E+00$
Cesium	$9.94E+01$	$3.13E+01$	$1.43E+01$	$1.71E+03$	$1.10E+03$	$9.66E+02$	$1.00E+00$

[a]Read as 1.97×10^4.

When considering the input parameters for the near-field transport, we must recall that the host rock in this environment is considered to be Topopah Spring welded tuff in the unsaturated zone (primarily the tsw35 hydro-geologic unit) and that transport occurs by molecular diffusion exclusively. The porosity and density of the near-field host rock are shown in Table V and are taken at their maximum, mean, and minimum values.[37] As discussed previously this diffusive transport will occur because the water contaminated with the radionuclides initially interfaces with the drift shadow region, a region in which advective transport is negligible.[22–24] The tortuosity correction factor in this is conservatively set to 1. Retardation effects due to sorption of radionuclides with the host rock are considered based on the mean of the distributions provided in the supporting documentation for the TSPA-LA.

When considering the far-field transport of radionuclides, we are concerned with transport in the fractures of the rock that composes the saturated zone. Transport calculations are particularly sensitive to the size of the fracture aperture. The supporting documentation for the TSPA-LA calculates the hydraulic fracture aperture 2*b* as the product of the flowing interval spacing and the flowing interval porosity. The flowing interval spacing is the distance between two segments in a bore sample that transmit significant amounts of water and is generally greater than the actual fracture spacing. We chose as our nominal case the mean value for the flowing interval spacing and, based on the distribution provided, set our minimum and maximum spacing two standards below

and above the mean, respectively. The value of the flowing interval porosity was fixed at its mean value. The values for the equilibrium sorption distribution coefficients are taken from the supporting documentation for the TSPA-LA for advective transport in the fractured volcanic rock matrix.[34]

V. NUMERICAL RESULTS

V.A. Results for Optimistic Far-Field Conditions

The results for the optimistic far-field environmental conditions provided above are not presented because the annual dose to the RMEI was observed to be too small to show in the ranges used in Figs. 12 through 16 in any of the four conditions studied (whole-element disposal and compact-only disposal in the fast and slow limits of graphite oxidation). Full compliance with Ref. 11 is observed; the annual dose to the RMEI remains below the regulatory threshold for geologic time periods with many orders of magnitude margin.

V.B. Results for Nominal Far-Field Conditions

Figure 12 shows the annual dose received by the RMEI in the nominal case, for compact-only disposal, in the fast graphite oxidation regime. This combination represents the highest dose to the RMEI among the four conditions in the nominal case. We can see that the DBSF meets the regulatory annual dose limit[11] to the RMEI in
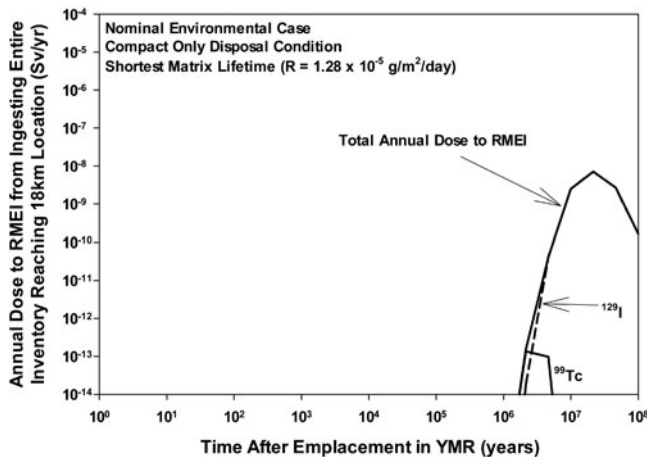
Fig. 12. Annual dose to the RMEI from the disposal of DBSF (nominal case with compact-only disposal condition in the fast graphite oxidation regime).

Fig. 13. Effect of waste matrix lifetime on the annual dose to the RMEI from the disposal of DBSF in the nominal case.

the million-year time frame. The annual dose actually has two peaks, the first of which is almost entirely due to ^{129}I between 10^7 and 10^8 yr, and the second of which is almost exclusively due to ^{227}Ac; ^{227}Ac is a decay daughter of ^{235}U (itself a decay daughter of ^{239}Pu), and the contribution to dose from ^{227}Ac is the result of ingrowth. The second peak annual dose is seen at 10^9 yr. This peak is not shown in Fig. 12 because of its extremely long time. The latter peak dose, 6.3×10^{-8} Sv/yr, remains well below the annual dose limit of 10^{-3} Sv/yr for the term between $10\,000$ and $1\,000\,000$ yr, indicating that under these conditions DBSF may pose negligible health risk even over geologic time periods.

Figure 13 shows the total annual dose to the RMEI in the nominal case for the four disposal conditions considered. We consider both the fast and the slow oxidation rates of the graphite waste matrix, and we consider the cases of whole-element disposal and compact-only disposal. These conditions provide a wide range in the projected lifetimes of the waste matrix. The effects of matrix lifetime are clear. By substantially extending the waste matrix lifetime, the overall annual dose to the RMEI is reduced. This results from the fact that all of the radionuclides, including the main contributor, ^{129}I, are released from the failed waste package congruently with the graphite matrix dissolution in each of these four conditions. Because of this congruency, given a greater matrix oxidation rate R, or a smaller graphite mass (compact only), the release rate of iodine increases, resulting in a higher dose rate at the downstream point.

An important retardation mechanism against the release of radionuclides to the biosphere is the diffusion of radionuclides out of the fracture and transport via diffusion into the volcanic rock matrix where the radionuclides are either sorbed into the host rock or
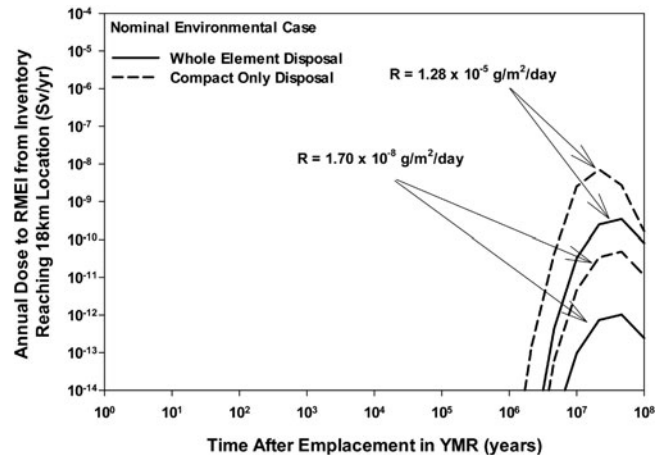
from which they will slowly diffuse back into the fracture. The effect of matrix diffusion was investigated by varying the matrix diffusion coefficient in the condition of compact-only disposal (low graphite mass), under fast graphite oxidation, in the nominal case given above. The value of the matrix diffusion coefficient was varied by an order of magnitude both above and below the mean value given in the supporting documents for the TSPA-LA. As seen in Fig. 14, the case of high matrix diffusion reveals a substantially reduced dose to the RMEI and highlights the importance of matrix diffusion in sequestering radionuclides from public exposure.
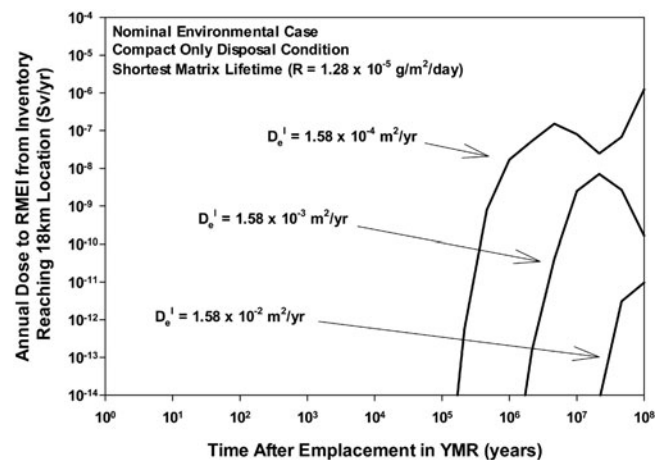

Fig. 14. Effect of matrix diffusion coefficient on the annual dose to the RMEI in the nominal case (compact-only disposal condition in the fast graphite oxidation regime).

V.C. Results for Pessimistic Far-Field Conditions

In all of the disposal conditions considered in the pessimistic case, all of the radionuclides are released congruently with the waste matrix. Figure 15 shows the results for the compact-only disposal, in the fast graphite oxidation regime, in the pessimistic case given above. We can see that even under these combinations the annual dose is observed to be less than the threshold set by Ref. 11 by nearly an order of magnitude. The total dose to the RMEI has two distinct peaks contributed to by several radionuclides. The earliest peak is largely due to ^{99}Tc (half-life 2.1×10^5 yr), followed by ^{237}Np (half-life 2.1×10^6 yr), which is almost entirely responsible for the highest peak. Again, ^{227}Ac provides the dose to the RMEI on the longest time frame. The relatively high annual dose delivered to the RMEI can be attributed to fast transport of radionuclides through large fractures and high solubilities assumed conservatively. The congruent release of radionuclides from the waste matrix implies that radionuclide concentrations will remain below their solubility limits for the duration of the radionuclide release from the waste matrix. This feature of DBSF performance confers a proportionality between the annual dose to the RMEI and the lifetime of the waste matrix. These results highlight the importance of geological, geochemical, and hydrogeological features in determining the potential health risk to the public from the disposal of high-level waste in a geological repository.

Figure 16 shows the effects of the graphite matrix lifetime, which is controlled by the initial mass of graphite and the corrosion rate R of graphite. Between the whole-element and the compact-only cases, the initial masses of graphite associated with each case are $4.93 \times$
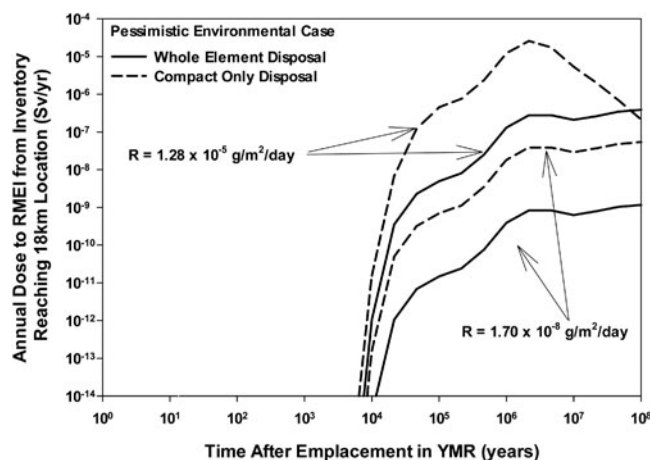
Fig. 16. Effect of waste matrix lifetime on the annual dose to the RMEI from the disposal of DBSF in the pessimistic case.

10^3 and 8.77×10^{-3} kg, respectively. This difference in mass translates into a proportional factor of approximately 100 difference in the transformed radii used in the lifetime calculation of the DBSF in the two disposal conditions (whole element and compact only) considered. This factor also appears proportionally as the difference between the dashed and solid curves for the same R value. Similarly, a factor of approximately 1000 difference in R appears as the difference by the same factor between the two solid curves and between the two dashed curves, respectively.

VI. DISCUSSION

For all the combinations studied, significant conservatism has been commonly implemented. It is assumed that radionuclides released from the entire repository are funneled into, confined in, and carried through the fictitious planar fracture pathway. The value of the solubility of each element in pore water in the diffusion barrier in the near-field region has been set at its upper-bound value in the assumed geochemical environment at the YMR. The package failure time has been assumed as only 1000 yr, which is factor of 1000 or greater more pessimistic than the assumption made in the TSPA-LA for the YMR. The protective roles of the drip shield and the transport time and the retardation effects in the unsaturated zone and the alluvium are all conservatively neglected.

We have considered 2 (mass of graphite matrix) $\times$ 2 (rate of graphite oxidation) $\times$ 3 (hydrogeological conditions in the far field) + 2 (matrix diffusion coefficients in the nominal case) = 14 combinations. Of these 14 combinations, four cases of the graphite-matrix conditions
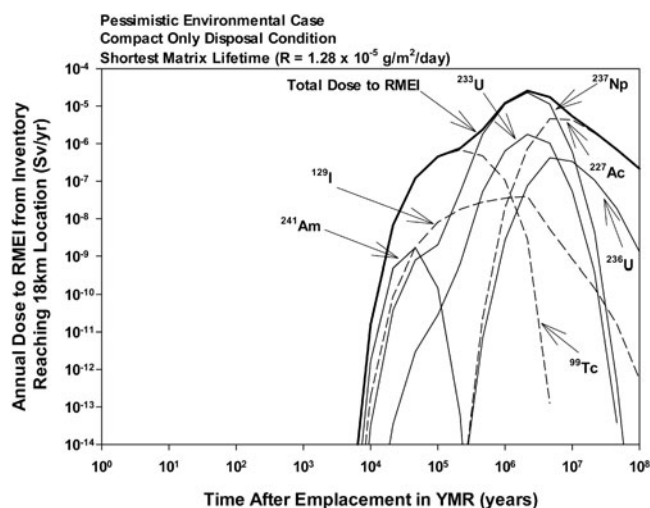
Fig. 15. Annual dose to the RMEI from the disposal of DBSF (pessimistic case with compact-only disposal condition in the fast graphite oxidation regime).

(mass and dissolution rate of graphite) under the optimistic far-field conditions have shown that the DBSF disposal would comply with the regulation with many orders of magnitude margin. Similar observations have been made for the cases under the nominal far-field conditions and even under the pessimistic far-field cases; the annual dose to the RMEI has been observed to comply with the regulatory limit in all cases studied. We have seen that compliance of the DBSF disposal in the YMR environment could be demonstrated thanks to the superior robustness of graphite and TRISO layers by a deterministic bounding analysis with high conservatism under the groundwater exposure scenario.

The graphite matrix plays an important role in retarding the release of radionuclides and sequestering them from the public. Parametric studies show a one-order-of-magnitude reduction in the dose to the RMEI for every order of magnitude extension in the lifetime of the fuel form. A significant portion of the radionuclide inventory, especially the shorter-lived fission products, decays within the graphite matrix before it has had a chance to be released and transported into either the near-field or far-field regions. If the dissolution rate of graphite is on the lower end of the range and the mass of graphite is large then, as Figure 16 shows, even in the pessimistic far-field case, DBSF would comply with the regulation with many orders of magnitude margin.

Long graphite lifetime makes the congruent release rate of radionuclides small, so that radionuclide concentrations at the graphite dissolution location become lower than their solubility limits. As many previous studies indicated, nuclide solubilities in geochemical conditions are greatly uncertain, resulting in significant uncertainty associated with the total repository performance. Therefore, with a robust waste form, such as graphite, the total system performance can be greatly improved as shown in this study and made more predictable, implying a need for more detailed material scientific studies on graphite as a waste form.

Further, it should be noted that the model presented in this paper for the performance of the DBSF, including the TRISO particles, as a waste form is applicable across a variety of repository conditions and geologies within the parameter ranges assumed in this study. The models for near- and far-field transport of radionuclides are also generic to any repository in which diffusive transport and advection through fracture networks are expected to be the dominant transport pathways.

VII. CONCLUSIONS

In the present paper, motivated by the observations made in previous studies that revealed superior robustness of graphite and TRISO layers in geological repository conditions, a deterministic bounding analysis has been performed to assess the annual dose to the RMEI by taking the Yucca Mountain conditions and comparing the results with the YMR performance standard given in Ref. 11.

Models have been developed for evaluating degradation rates of graphite and TRISO layers based on previous experimental studies. Based on the observation from the model evaluation that graphite dissolution is the rate-limiting process, the radionuclide release model has been developed and used as the source term for the far-field transport calculation. The existing computer code TTB has been utilized to perform the actual computation, which utilizes numerical inversion of Laplace transformed analytical solutions for transport of a multimember decay chain. Radionuclide composition in TRISO particles has been evaluated by the MOCUP code. Solubility of actinide elements in the Yucca Mountain environment with modification of carbon dioxide fugacity was obtained by PHREEQC simulation code. Various data for repository configurations and hydrogeological parameters were referenced from the TSPA-LA report.

The results of the present deterministic performance assessment show the following:

1. All of the cases of the groundwater exposure pathway that have been investigated in this paper, including the optimistic, nominal, and pessimistic cases, have indicated compliance with the regulatory limit for the annual dose to the RMEI, with orders of magnitude margins, despite numerous conservative assumptions. In the nominal case the major contributor to the annual dose is ^{129}I; other nuclides decay out before they reach the intake point located 18 km downstream from the repository. Under the pessimistic case the major contributors to the annual dose are ^{99}Tc, ^{237}Np, and ^{227}Ac; high-flow conditions in large fractures coupled with high radionuclide solubilities lead to rapid transport of these radionuclides to the observation point.

2. With the assumed high durability of graphite, in all of the cases studied, all radionuclides are released congruently with graphite corrosion. This congruency results in nearly linear dependency of the annual dose to the RMEI on the graphite lifetime. Congruency also implies that radionuclide concentrations in groundwater are smaller than their solubility limits, resulting in low annual dose to the RMEI. This highlights the possibility and advantage of the use of graphite as a waste matrix for the disposal of high-level waste and the need for detailed material scientific studies on the mechanisms of graphite corrosion in repository environments.

3. Finally, it must be noted that many of the parameters used are associated with aleatory and epistemic uncertainties. To make a more effective assessment of the potential health risk to the public from the disposal of DBSF in the YMR, we must make a probabilistic sampling of the parameter space. Additionally, alternate

pathways for exposure must be investigated in order to conclusively determine compliance with regulatory standards. This is the focus of ongoing research.

REFERENCES

1. M. RICHARDS, "Assessment of GT-MHR Spent Fuel Characteristics and Repository Performance," PC-000502, Rev. 0, General Atomics (Apr. 2002)

2. C. RODRIGUEZ et al., "Deep-Burn: Making Nuclear Waste Transmutation Practical," *Nucl. Eng. Des.*, **222** (2003).

3. M. RICHARDS et al., "Deep Burn: Destruction of Nuclear Waste Using MHR Technology—Impact on Spent Fuel Management," *Proc. GLOBAL 2005*, Tsukuba, Japan, October 9–13, 2005, Paper 313.

4. J. AHN et al., "The Repository Performance of Spent TRISO Fuel," *Proc. HTR 2010*, Prague, Czech Republic, October 18–20, 2010, Paper 098.

5. M. FRATONI, "Development and Applications of Methodologies for the Neutronic Design of the Pebble Bed Advanced High Temperature Reactor (PB-AHTR)," PhD Dissertation, University of California, Berkeley (2008).

6. W. J. GRAY, "A Study of the Oxidation of Graphite in Liquid Water for Radioactive Storage Applications," *Radioact. Waste Manage. Nucl. Fuel Cycle*, **3**, *2*, 137 (1982).

7. J. FACHINGER et al., "Behaviour of Spent HTR Fuel Elements in Aquatic Phases of Repository Host Rock Formations," *Nucl. Eng. Des.*, **236**, *5–6*, 543 (2006).

8. A. L. LOTTS et al., "Options for Treating High-Temperature Gas-Cooled Reactor Fuel for Repository Disposal," ORNL/TM-12077, Oak Ridge National Laboratory (1992).

9. E. MORRIS and T. BAUER, "Modeling of the Repository Behavior of TRISO Fuel," ANL-AFCI-160, Argonne National Laboratory (Sep. 2005).

10. J. L. PETERSON and M. L. DUNZIK-GOUGAR, "Modeling Spent TRISO Fuel for Geological Disposal: Corrosion and Failure Under Oxidizing Conditions in the Presence of Water," *Prog. Nucl. Energy*, **53**, *3*, 278 (2011).

11. *Code of Federal Regulations*, Title 40, "Protection of Environment," Part 197, "Public Health and Environmental Radiation Protection Standards for Yucca Mountain, Nevada," Environmental Protection Agency (2012).

12. *Waste Forms Technology and Performance: Final Report*, Committee on Waste Forms Technology and Performance, Nuclear Radiation Studies Board, National Research Council, National Academies, National Academies Press (2011).

13. J. AHN, "Integrated Radionuclide Transport Model for a High-Level Waste Repository in Water-Saturated Geologic Formations," *Nucl. Technol.*, **121**, 24 (1998).

14. "Radionuclide Screening," ANL-WIS-MD-000006, Rev. 02, Sandia National Laboratories, U.S. Department of Energy Office of Civilian Radioactive Waste Management (2007).

15. R. L. MOORE, B. G. SCHNITZLER, and C. A. WEMPLE, "MOCUP: MCNP-ORIGEN2 Coupled Utility Program," INEL-95/0523, Idaho National Engineering Laboratory (1995).

16. X-5 MONTE CARLO TEAM, "MCNP—A General Monte Carlo N-Particle Transport Code, Version 5," Los Alamos National Laboratory (2003).

17. A. G. CROFF, "ORIGEN2: A Versatile Computer Code for Calculating the Nuclide Compositions and Characteristics of Nuclear Materials," *Nucl. Technol.*, **62**, 335 (1983).

18. M. FRATONI and E. GREENSPAN, "Determination of the Equilibrium Composition of Cores with Continuous Fuel Feed and Removal Using MOCUP," *Proc. Joint Int. Topl. Mtg. Mathematics & Computation and Supercomputing in Nuclear Applications*, Monterey, California, April 15–19, 2007, American Nuclear Society (2007).

19. J. F. ESPINAL, F. MONDRAGON, and T. N. TRUONG, "Thermodynamic Evaluation of Steam Gasification Mechanisms of Carbonaceous Materials," *Carbon*, **47**, *13*, 3010 (2009).

20. L. L. SNEAD et al., "Handbook of SiC Properties for Fuel Performance Modeling," *J. Nucl. Mater.*, **371**, *1–3*, 329 (2007).

21. "Total System Performance Assessment Model/Analysis for the License Application," MDL-WIS-PA-000005, Rev. 00, Sandia National Laboratories, U.S. Department of Energy Office of Civilian Radioactive Waste Management (2008).

22. J. R. PHILIP, J. H. KNIGHT, and R. T. WAECHTER, "Unsaturated Seepage and Subterranean Holes: Conspectus, and Exclusion Problem for Circular Cylindrical Cavities," *Water Resour. Res.*, **25**, *1*, 16 (1989).

23. J. E. HOUSEWORTH, S. FINSTERLE, and G. S. BODVARSSON, "Flow and Transport in the Drift Shadow in a Dual-Continuum Model," *J. Contam. Hydrol.*, **62–63**, 133 (2003).

24. "Yucca Mountain Science and Engineering Report," DOE/RW-0539-1, U.S. Department of Energy Office of Civilian Radioactive Waste Management (Feb. 2002).

25. Y. WU, "UZ Flow Models and Submodels," MDL-NBS-HS-000006, Rev. 02, U.S. Department of Energy Office of Civilian Radioactive Waste Management (2004).

26. B. W. ARNOLD, "Saturated Zone Flow and Transport Model Abstraction," MDL-NBS-HS-000011, Rev. 03, U.S. Department of Energy Office of Civilian Radioactive Waste Management (2005).

27. S. KELLER, "Site-Scale Saturated Zone Transport," MDL-NBS-HS-000010, Rev. 02, U.S. Department of Energy Office of Civilian Radioactive Waste Management (2004).

28. D. W. WU, "Biosphere Model Report," MDL-MGR-MD-000001, Rev. 00, U.S. Department of Energy Office of Civilian Radioactive Waste Management (2003).

29. J. AHN, "Environmental Impact of Yucca Mountain Repository in the Case of Canister Failure," *Nucl. Technol.*, **157**, 87 (2007).

30. "Final Environmental Impact Statement for a Geologic Repository for the Disposal of Spent Nuclear Fuel and High-Level Radioactive Waste at Yucca Mountain, Nye County, Nevada," DOE/EIS-0250, Appendix A, U.S. Department of Energy Office of Civilian Radioactive Waste Management (Feb. 2002).

31. D. L. PARKHURST and C. A. J. APPELO, "User's Guide to PHREEQC, Version 2," Water Resource Investigations Report 99-4259, U.S. Geological Survey (1999).

32. B. P. VAN DEN AKKER and J. AHN, "Solubilities of Radionuclides Released from Graphite Waste Calculated Using PHREEQC," *Proc. 13th Int. High-Level Radioactive Waste Management Conf.*, Albuquerque, New Mexico, April 10–14, 2011, American Nuclear Society (2011).

33. P. BERNOT, "Dissolved Concentration Limits of Elements with Radioactive Isotopes," ANL-WIS-MD-000010, Rev. 06, U.S. Department of Energy Office of Civilian Radioactive Waste Management (2007).

34. P. W. REIMUS, "Saturated Zone In-Situ Testing," ANL-NBS-HS-000039, Rev. 01, U.S. Department of Energy Office of Civilian Radioactive Waste Management (2004).

35. B. ROBINSON, "Particle Tracking Model and Abstraction of Transport Processes," MDL-NBS-HS-000020, Rev. 01, U.S. Department of Energy Office of Civilian Radioactive Waste Management (2004).

36. S. KUZIO, "Probability Distribution for Flowing Interval Spacing," ANL-NBS-MD-000003, Rev. 01, U.S. Department of Energy Office of Civilian Radioactive Waste Management (2004).

37. H. LIU, "Calibrated Unsaturated Zone Properties," ANL-NBS-HS-000058, Rev. 00, U.S. Department of Energy Office of Civilian Radioactive Waste Management (2007).